Dual-Stage Actuator Control Design Using a Doubly Coprime Factorization Approach

Jinchuan Zheng, Weizhou Su, and Minyue Fu, *Fellow, IEEE*

***Abstract*—This paper first reveals that the tracking and disturbance rejection problems can be decoupled into two independent optimization problems under the 2-DOF control framework. This result is then used for the design of a 2-DOF controller for a dual-stage actuator (DSA) system to provide desired performance of disturbance rejection and step tracking. The 2-DOF controller is designed based on the doubly coprime factorization approach, with which the closed-loop transfer function is expressed explicitly in terms of design parameters. This greatly simplifies the optimization of design parameters in meeting desired specifications. We further study how to use the design parameters to deal with specific problems in the DSA, i.e., control allocation and trajectory planning. For step tracking beyond the secondary actuator range, a nonlinear controller is also used for the primary actuator to complete the task. Experimental results demonstrate the practical implementation of the DSA control system and verify its effectiveness for step tracking and disturbance rejection and its robust performance under load changes.**

***Index Terms*—Doubly coprime factorization (DCF), dual-stage actuator (DSA), motion control, 2-DOF control.**

I. Introduction

DUAL-STAGE actuator (DSA) servo systems are characterized by a structural design with two actuators connected in series along a common axis. The primary actuator (coarse actuator) is of long travel range but with poor accuracy and slow response time. The secondary actuator (fine actuator) is typically of higher precision and faster response but with a limited travel range. By combining the DSA system with a properly designed servo controller, the two actuators are complementary to each other providing long travel range, high positioning accuracy, and fast response. The DSA servomechanism has been commonly used in the industry, e.g., the dual-stage hard disk drive (HDD) actuator [1]–[3]. The dual-stage HDD servomechanism can significantly increase the servo bandwidth to lower the sensitivity to various disturbances, and thus, push the track density [4]. Other DSA applications also include machine tools [5], robot manipulators [6], XY positioning tables [7], nanopositioner [8], and DSAs using stick–slip [9], [10] or inchworm actuators [11].

Manuscript received October 1, 2008; revised March 25, 2009. First published July 14, 2009; current version published April 2, 2010. Recommended by Technical Editor O. Kaynak. This work was supported in part by a Research Grant from The University of Newcastle, Australia, and in part by the Natural Science Foundation of China under Grant 60834003 and Grant 60774057.

J. Zheng and M. Fu are with the School of Electrical Engineering and Computer Science, The University of Newcastle, Newcastle, NSW 2308, Australia (e-mail: jinchuan.zheng@newcastle.edu.au; minyue.fu@newcastle.edu.au).

W. Su is with the College of Automation Science and Engineering, South China University of Technology, Guangzhou 510641, China (e-mail: wzhsu@scut.edu.cn).

Digital Object Identifier 10.1109/TMECH.2009.2025772

Although the mechanical design of a DSA system appears to be simple, it is a challenging task to design controllers for the two actuators to yield an optimal performance because of the specific characteristics in the DSA systems. 1) The DSA system is a dual-input single-output (DISO) system, which means that for a given desired trajectory, inputs to the two actuators are not unique. Thus, a proper control strategy is required for control allocation. 2) The secondary actuator typically has a very limited travel range, which results in a severe actuator saturation problem. A number of approaches have been reported to deal with dual-stage control problems. Control design for reference following can be found in [12]–[14]. The secondary actuator saturation problem is explicitly taken into account in [15] and [16] during the control design. A decoupled track-seeking controller is developed in [17] to enable high-speed short-span seeking for a dual-stage HDD servo system. Further, short- and long-span seeking controls are incorporated in a single control scheme with fast settling time [18], [19]. The literature has also demonstrated successful applications of some new control theories and design methods to DSA servo systems. For example, robust control is used to overcome plant uncertainty and maintain performance [7], [13]. Repetitive control is used to suppress periodic disturbances and vibrations [5]. Nonlinear control is applied to handle the actuator saturation [18] or to enhance the seeking performance [19].

In this paper, we present a new control design method for a DSA system consisting of a linear motor (LM) and a piezoactuator (PA). We focus on the development of a two-degree-of-freedom (2-DOF) controller for disturbance rejection and step tracking in the PA range. A doubly coprime factorization (DCF) [20] is used for the 2-DOF controller design because it can provide the advantages that: 1) it parameterizes all linear internally stabilized 2-DOF controller by two free design parameters; 2) it offers a unifying design method to solve the tracking and disturbance rejection problems; and 3) the derived frequency transfer functions of disturbance rejection response and seeking response are simply expressed and they are uniquely in terms of the design parameters, which makes the relationship between the design parameters and the desired specifications explicit. Compared with the existing DSA control methods, the proposed 2-DOF controller in this paper explicitly addresses both the step tracking and disturbance rejection problems in a unifying design framework and gives a solution to a specified performance index indicating the tracking performance. Further, we reveal that the tracking performance of asymptotical tracking and disturbance rejection in the dual-stage systems is equivalent to two independent optimization problems. This result obviously can decouple the design goals for such a

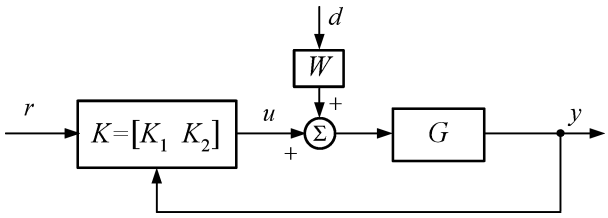

Fig. 1. Generic 2-DOF control system.

multiobjective design problem, and thus, simplify the control design process. To complete the functionality of the DSA, a nonlinear controller is also introduced for the LM to achieve step tracking beyond the PA range. Therefore, the resulting DSA control system involves both linear control and nonlinear control, where linear control (i.e., 2-DOF control) is used for local control only. Finally, we verify the effectiveness of the DSA controller through experimental results.

Throughout this paper, we use the following notation. For any signal $u(t)$, we denote its Laplace transform by $\hat{u}(s)$. $\|\cdot\|$ denotes the Euclidean vector norm and $\|\cdot\|_2$ the norm in space L_2. Let $\mathcal{R}H_\infty$ denote the set of all stable, proper, and rational transfer function matrices.

II. 2-DOF Control Design Based on DCF

The 2-DOF control systems are the most general feedback configuration in linear control schemes. Fig. 1 shows a generic structure for this class of systems. In this setup, G denotes the given linear time-invariant (LTI) plant model, W denotes the known LTI stable and proper weight, and K denotes the 2-DOF controller to be designed. The signals r, y, u, and d represent, respectively, the step reference signal, the system output, the control input, and the disturbance with energy bounded by δ^2, i.e., $\|d\|_2^2 \le \delta^2$.

In this paper, we consider the asymptotic tracking and disturbance rejection problems for the system in Fig. 1. We need to design the controller K such that the closed-loop system is internally stable and the system output y asymptotically tracks a step signal $r(t) = v$, $t \ge 0$, for all disturbance $d \in L_2$ with $\|d\|_2 \le \delta$. The measure of the tracking performance is defined as

$$J = \int_0^\infty \|e(t)\|^2 dt \tag{1}$$

where $e(t) = r(t) - y(t)$ denotes the tracking error. Obviously, J depends on the disturbance d. We thus consider the worst value of J over all possible d as the performance index for the tracking and disturbance rejection problems, i.e.,

$$\sup_{\|d\|_2 \le \delta} J. \tag{2}$$

Therefore, it is our interest to seek a controller K among all possible stabilizing 2-DOF controllers to achieve the minimum value of (2) defined by

$$J_{\text{opt}} = \inf_K \sup_{\|d\|_2 \le \delta} J. \tag{3}$$

The DCF is a well-suited approach to solve (3). Let the right and left coprime factorizations of G be given by

$$G = ND^{-1} = \tilde{D}^{-1}\tilde{N} \tag{4}$$

where N, D, $\tilde{N}$, $\tilde{D} \in \mathcal{R}H_\infty$ and satisfy the doubly Bezout identity

$$\begin{bmatrix} \tilde{X} & -\tilde{Y} \\ -\tilde{N} & \tilde{D} \end{bmatrix} \begin{bmatrix} D & Y \\ N & X \end{bmatrix} = I \tag{5}$$

for some $X, Y, \tilde{X}, \tilde{Y} \in \mathcal{R}H_\infty$.

Nett *et al.* [21] have proposed explicit formulas for the DCF representation of an LTI system in terms of its state-space realization. This method is numerically easy to use. To do this, we first represent the plant model $G(s)$ in state space as follows:

$$G(s) = C(sI - A)^{-1}B \tag{6}$$

where A, B, and C are matrices with appropriate dimensions. Suppose the pairs (A, B) and (A, C) are stabilizable and detectable, respectively. Select F and L such that $(A - BF)$ and $(A - LC)$ are both Hurwitz. Thus, a DCF of $G(s)$ is given by

$$\begin{cases} N(s) = C(sI - A + BF)^{-1}B \\ D(s) = I - F(sI - A + BF)^{-1}B \\ \tilde{N}(s) = C(sI - A + LC)^{-1}B \\ \tilde{D}(s) = I - C(sI - A + LC)^{-1}L \\ X(s) = I + C(sI - A + BF)^{-1}L \\ \tilde{X}(s) = I + F(sI - A + LC)^{-1}B \\ Y(s) = -F(sI - A + BF)^{-1}L \\ \tilde{Y}(s) = -F(sI - A + LC)^{-1}L. \end{cases} \tag{7}$$

According to [20], the class of all linear internally stabilizing 2-DOF controllers $K = [K_1 \;\; K_2]$ can be parameterized by

$$\hat{u} = K_1\hat{r} + K_2\hat{y} \tag{8}$$

$$K_1 = (\tilde{X} - R\tilde{N})^{-1}Q \tag{9}$$

$$K_2 = (\tilde{X} - R\tilde{N})^{-1}(\tilde{Y} - R\tilde{D})$$

$$Q, R \in \mathcal{R}H_\infty \tag{10}$$

where Q and R are the free parameters to be designed. By substituting the controllers K_1, K_2, and the factorized plant model (4) into Fig. 1, we can easily obtain the following input–output relationship in the frequency domain:

$$\hat{y} = T_{yr}\hat{r} + T_{yd}\hat{d} \tag{11}$$

with

$$T_{yr} = NQ \tag{12}$$

$$T_{yd} = (X - NR)\tilde{N}W \tag{13}$$

where T_{yr} and T_{yd} denote the closed-loop transfer functions from the reference and disturbance to the system output, respectively. The proof of the formulas (12) and (13) is given in the Appendix. It is advantageous that the closed-loop transfer functions are expressed by the design parameters Q and R

explicitly. Hence, from Parseval's theorem, we have

$$J = \int_0^\infty \|e(t)\|^2 dt = \|\hat{r} - \hat{y}\|_2^2$$
$$= \|(I - T_{yr})\hat{r} - T_{yd}\hat{d}\|_2^2. \quad (14)$$

Then, the following result is clear.

Theorem 1 [22]: Let G have nonminimum phase (NMP) zeros $z_1, z_2, \ldots, z_m$ with corresponding Blaschke vectors $\eta_1, \eta_2, \ldots, \eta_m$. Then, the minimax tracking performance of asymptotical tracking and disturbance rejection of the system is given by

$$J_{\text{opt}} = \inf_Q \|(I - T_{yr})\hat{r}\|_2^2 + \delta^2 \inf_R \|T_{yd}\|_\infty^2 \quad (15)$$

$$= 2\sum_{i=1}^{m} \frac{\text{Re}(z_i)}{|z_i|^2} \cos^2 \angle(\eta_i, v) + \delta^2 \inf_R \|T_{yd}\|_\infty^2. \quad (16)$$

Remark 1: The theorem reveals that the optimal tracking performance with the 2-DOF controller is a sum of two terms as shown in (15). The first term is the optimal tracking performance of the system without the disturbance input d, while the second one is the best achievable performance of disturbance attenuation of the system without the reference signal r. These two optimal problems have been studied in [23] and [24], respectively; the results therein are then applied to yield (16).

From the controller design point of view, Theorem 1 also implies that to achieve J_{opt} is equivalent to two independent optimization problems in terms of the free parameters R and Q, respectively. More specifically, these two problems are as follows.

1) Design $R \in \mathcal{R}H_\infty$ to minimize $\|(X - NR)\tilde{N}W\|_\infty$.
2) Design $Q \in \mathcal{R}H_\infty$ to minimize $\|(I - NQ)\hat{r}\|_2^2$.

Intuitively, one may simply choose $R = N^{-1}X$ and $Q = N^{-1}$ to yield $J_{\text{opt}} = 0$. However, this option only applies to the special case where the plant must be proper, right invertible, stable and minimum phase, the resulting R and Q are proper, and the control input has no saturation. In practical servomechanisms, these strict conditions are rarely satisfied at the same time. Instead, the designer has to deal with one or more of these constraints. Therefore, the design of R and Q requires some extra techniques to obtain a practical servo system without degrading the tracking performance significantly. In general, we can attempt to design R and Q such that $T_{yd} = (X - NR)\tilde{N}W \to 0$ and $T_{yr} = NQ \to I$ in the frequency of interest according to the design specifications [25]. Under this circumstance, a suboptimal controller is achieved to approximate the optimal one that yields (16), while to handle the constraints at hand. The performance of the resulting servo system will then compromise among the optimal tracking, robustness, and easy implementation (e.g., least controller order). The design examples along this line include [26] that aims for optimal step responses of a unstable and NMP flexible beam, and [27] that handles control design with actuator torque constraints.

In the next section, we will apply such a 2-DOF controller design approach to a DSA servo system, which consists of a DISO plant with saturations for both actuators. In particular, we will address the design of R that determines the control allocation of the two actuators for disturbance rejection and the robust stability of the feedback loop. On the other hand, Q is designed to generate the desired trajectories in response to a step reference for the two actuators; as such, the overall system output can obtain a fast and smooth response.

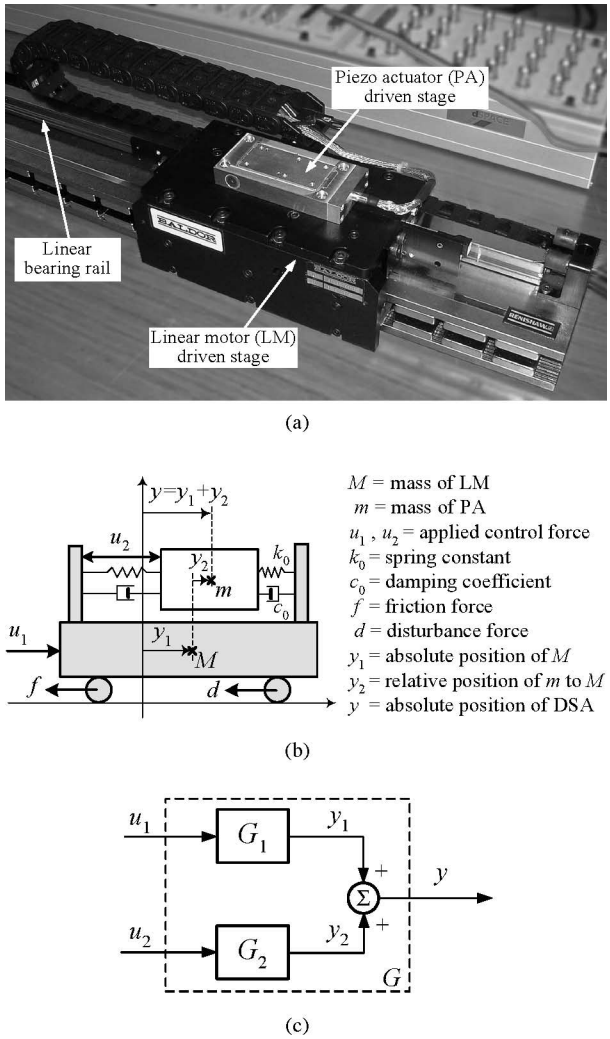

Fig. 2. DSA positioning system. (a) Experimental setup. (b) Illustration of the DSA. (c) DISO plant model of the DSA (G_1: LM model, G_2: PA model).

III. Application to a DSA Control System

A. Plant Modeling

The DSA positioning system is depicted in Fig. 2(a), which consists of a primary stage driven by an LM and a secondary stage driven by a PA. The LM has a 0.5-m travel range, while the PA has a limited travel range of ± 15 μm. Fig. 2(b) illustrates the mechanical structure of the DSA. The nonlinear friction force f of the LM is overcome by a precompensator (see [19] for details). The PA is equipped with integrated control electronics, which eliminates the piezoceramics nonlinearities such as hysteresis and creep providing linearity up to 3 nm. Additionally, the control electronics actively damps the mechanical resonance of the PA stage flexure. In this setup, we can simply ignore the coupling forces between the two actuators mainly because of the much larger mass of the LM relative to the PA

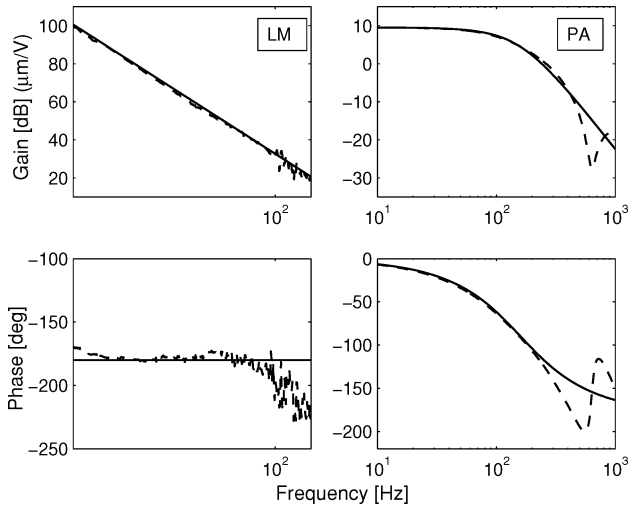

Fig. 3. Frequency responses of the DSA system (solid lines: identified, dashed lines: measured).

and the high stiffness of the PA. For more details of justification of this approximation, see [19]. After these manipulations, the control-oriented DSA plant model can be depicted by Fig. 2(c). The LM model is approximated by

$$G_1 = \frac{\hat{y}_1}{\hat{u}_1} = \frac{k_1}{s^2} \tag{17}$$

where y_1 is the LM position output, u_1 is the control input with $|u_1| \le \bar{u}_1 = 1$ V, and $k_1 = 1.5 \times 10^7$. The PA model is approximated by

$$G_2 = \frac{\hat{y}_2}{\hat{u}_2} = \frac{k_2}{s^2 + as + b} \tag{18}$$

where y_2 is the PA position output relative to the LM, u_2 is the control input with $|u_2| \le \bar{u}_2 = 5$ V, and $k_2 = 3.0 \times 10^6$, $a = 1810$, and $b = 1.0 \times 10^6$. Fig. 3 shows the frequency responses of the LM and PA system, which verify the accuracy of the identified models in the frequency of interest [19].

In Fig. 2(c), the system output y, i.e., the absolute position of the PA, is the only available measured output for feedback control. Hence, the overall DSA model G can be represented as a DISO linear system

$$\hat{y} = G\hat{u} = [G_1 \;\; G_2] \begin{bmatrix} \hat{u}_1 \\ \hat{u}_2 \end{bmatrix}. \tag{19}$$

To obtain the DCF of G by (7), we transform G into a state-space form as (6), whose system matrices are given by

$$A = \left[\begin{array}{c|c} A_1 & 0 \\ \hline 0 & A_2 \end{array}\right] = \left[\begin{array}{cc|cc} 0 & 1 & 0 & 0 \\ 0 & 0 & 0 & 0 \\ \hline 0 & 0 & 0 & 1 \\ 0 & 0 & -b & -a \end{array}\right]$$

$$B = \left[\begin{array}{c|c} B_1 & 0 \\ \hline 0 & B_2 \end{array}\right] = \left[\begin{array}{c|c} 0 & 0 \\ k_1 & 0 \\ \hline 0 & 1 \\ 0 & k_2 \end{array}\right]$$

$$C = [\, C_1 \;\; | \;\; C_2 \,] = [\, 1 \;\; 0 \;\; | \;\; 1 \;\; 0 \,]$$

where $A_{1,2}$, $B_{1,2}$, and $C_{1,2}$ are the state-space representation of the LM and PA, respectively.

For the disturbance source, we are concerned with a shock disturbance acting on the LM. The half-sine wave with a duration of 10 ms is typically used as the standard industry shock test [28]. Thus, we can model the disturbance as

$$W = \begin{bmatrix} \dfrac{0.05}{0.0008s + 1} \\ 0 \end{bmatrix}$$

$$d = \begin{cases} \sin(314(t - t_0)), & t \in [t_0,\ t_0 + 0.01] \\ 0, & \text{otherwise} \end{cases}$$

where t_0 denotes the time instance at which the disturbance is injected. Obviously, we have $\|d\|_2 \le \delta = 0.0707$.

In the sequel, we first present the 2-DOF controller design for step responses within the PA range, and then, discuss a switching control scheme to incorporate the step responses beyond the PA range.

B. 2-DOF Controller for Step Response Within PA Range

The 2-DOF controller for the DSA step responses within the PA range should satisfy the following specifications.

1) The overshoot should be kept under 1 μm.
2) The control inputs to the LM and PA are not saturated, i.e., should not exceed ± 1 and ± 5 V, respectively.
3) In response to a step reference, the displacement of PA should settle down to zero at steady state such that it can further response to a sequential step reference.
4) The DSA servo system should have gain margin (GM) larger than 6 dB and phase margin (PM) more than 50°.

For simplicity, we will present a step-by-step design procedure.

Step 1: DCF of G

According to (7), we should first select F and L such that $(A - BF)$ and $(A - LC)$ are both Hurwitz. Clearly, F is a state-feedback gain matrix and L is a state-estimator gain matrix. Since there is no coupling between the LM and the PA, the gains F and L can be partitioned as

$$F = \left[\begin{array}{c|c} F_1 & 0 \\ \hline 0 & F_2 \end{array}\right] \qquad L = \left[\begin{array}{c} L_1 \\ \hline L_2 \end{array}\right]. \tag{20}$$

Hence, we can individually design the gains for the LM and PA loops by using the pole placement method such that the PA loop should have a faster dynamics than the LM loop, and the estimator is faster than the state feedback loop. To do this, we select $F_1 = [0.0024 \;\; 2.2 \times 10^{-5}]$ and $L_1 = [3037 \;\; 3.8 \times 10^6]^T$ to make the LM loop and its estimator have a bandwidth of 30 and 200 Hz, respectively, and select $F_2 = -[0.286 \;\; 3.7 \times 10^{-4}]$ and $L_2 = [243 \;\; -3.6 \times 10^5]^T$ for the counterparts of the PA with 60 and 250 Hz bandwidths, respectively. Then, the DCF of G can be easily computed by (7).

Step 2: Design of R

For disturbance rejection, we should make the disturbance rejection function $T_{yd} = (X - NR)\tilde{N}W \to 0$ in the low frequencies. Let $R = [R_1 \;\; R_2]^T$ and $N = [N_1 \;\; N_2]$, we then take

$$R_1 = N_1^{-1} X r_1(s) \tag{21}$$

$$R_2 = N_2^{-1} X r_2(s) \tag{22}$$

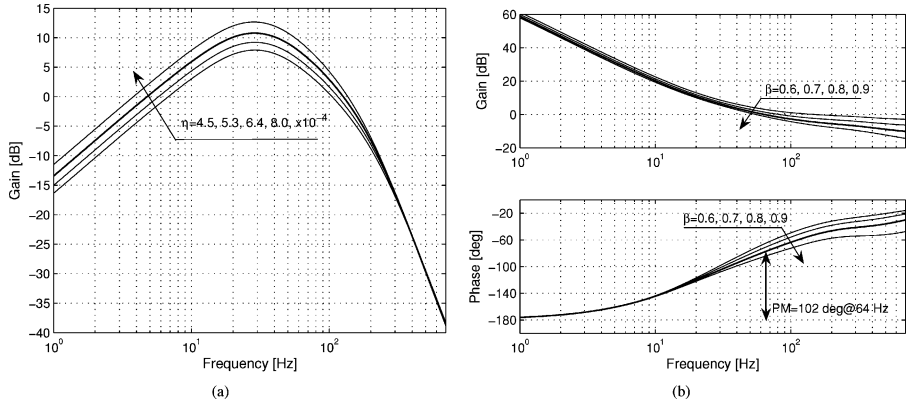

Fig. 4. Bode plots. (a) Disturbance rejection response T_{yd}. (b) Γ function indicating DSA control allocation ($\eta = 6.4 \times 10^{-4}$).

with

$$r_1(s) = \frac{1-\beta}{(\eta s+1)^2} \tag{23}$$

$$r_2(s) = \frac{\beta}{(\eta s+1)^2} \tag{24}$$

where $\eta > 0$ and $\beta \in [0 \;\; 1]$ are tuning scalars. Note that the order of $r_{1,2}$ is chosen to make $R_{1,2}$ proper at least. Further, we can see that $R_{1,2}$ is stable because, in our case, X is stable and $N_{1,2}$ has no NMP zeros, respectively. Then, we have

$$T_{yd} = \left(1 - \frac{1}{(\eta s+1)^2}\right) X\tilde{N}W. \tag{25}$$

We can see that the term $(1 - 1/(\eta s+1)^2)$ introduces low gains in low frequencies for disturbance rejection. Moreover, the available frequency region for the disturbance rejection problem can be increased with a smaller η, as shown in Fig. 4 (a). Ideally, the system stability can be guaranteed with an arbitrary η, which, however, may not preserve a desired stability margin. To see this, we can study the DSA open-loop characteristics, which is defined by

$$OL(s) = GK_2 = \frac{Y_1G_1 + Y_2G_2 - X/(\eta s+1)^2}{X(1-1/(\eta s+1)^2)} \tag{26}$$

where Y_1 and Y_2 are, respectively, the elements of Y with $Y = [Y_1 \;\; Y_2]^T$. It is clear that the open-loop transfer function is related to η only. However, the relationship between the stability margin and η is implicit. Hence, we may have to tune η by trial and error such that the desired disturbance rejection function in (25) and stability margin are both achieved.

Next, we discuss how to select β. In fact, for a given T_{yd} (or equivalently, a given position output), β is related to the allocation of the control efforts of the two actuators. Typically, the LM works mainly for the low-frequency movement, while the PA responses more for high-frequency disturbance. With such allocation in the frequency domain, it is possible to take full advantage of the PA to bypass the LM uncertainty in the high-frequency band and improve the servo bandwidth. A key point to analyze the control allocation of the two actuators is the intersection of the two paths in the frequency domain. Specifically, we can analyze the ratio of the open-loop systems of the two

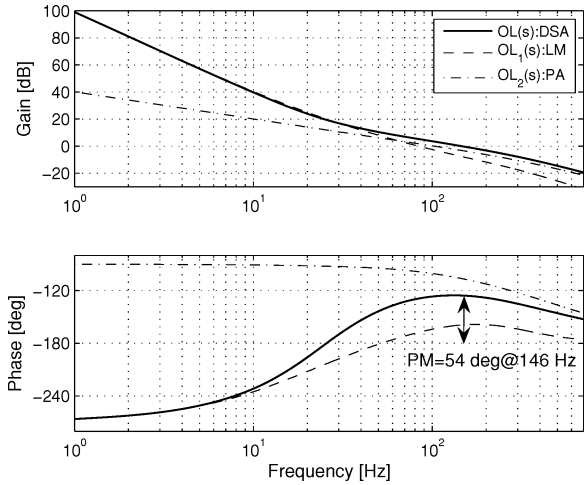

Fig. 5. Bode plot of DSA open-loop systems indicating stability margin.

actuators. This idea is identical to the so-called PQ method [12]. Let the controller $K_2 = [K_{21} \;\; K_{22}]^T$, and then, define the open-loop systems of the LM and PA as $OL_1 = G_1K_{21}$ and $OL_2 = G_2K_{22}$, respectively. Then, we can obtain the ratio of OL_1 and OL_2 as

$$\Gamma = \frac{OL_1}{OL_2} = \frac{X(1-\beta) - (\eta s+1)^2Y_1G_1}{X\beta - (\eta s+1)^2Y_2G_2}. \tag{27}$$

We can see that Γ is a function of β provided that η is determined. In order to make the two actuators have maximum cooperation, Γ is chosen to give a roll-off characteristics and a PM of at least 60° at the 0-dB crossover frequency [12].

In our case, we choose $\eta = 6.4 \times 10^{-4}$, and the corresponding Bode plot of the T_{yd} is shown in Fig. 4(a). Based on (27), we then choose $\beta = 0.8$, which achieves a PM of 102° for Γ function, as shown in Fig. 4(b), from which we can also see that the 0-dB crossover frequency (also referred to as the hand-off frequency) decreases with a larger β. This indicates a large disturbance rejection contribution from the PA, but it also tends to saturate the PA. To check the stability margin, Fig. 5 shows the open-loop system of the DSA, which indicates that the DSA open-loop system $[OL(s)]$ is dominated by the LM loop $[OL_1(s)]$ in the low frequency while by the PA loop

$[OL_2(s)]$ in the high frequency. Furthermore, the DSA system achieves a PM of 54° at 146 Hz and a GM of ∞. Compared with the LM loop whose PM is only 13° at 84 Hz, we can see that the PA loop improves the stability margin and pushes the open-loop frequency bandwidth.

Step 3: Design of Q

Let $Q = [Q_1 \quad Q_2]^T$. Due to the fact that G_1 and G_2 are minimum phase, we thus aim at the design of Q_1 and Q_2 such that $T_{yr} = N_1Q_1 + N_2Q_2 \to 1$ has a high-frequency bandwidth and the control inputs for a step response are within both actuators' control limits. Furthermore, it is required that the displacement of PA settles down to zero at steady state. This means that $y_1(\infty) = r$ and $y_2(\infty) = 0$ should be satisfied for a step response with amplitude r assuming the disturbance with $d(\infty) = 0$. Hence, we first analyze the individual position outputs of the two actuators. Partition D is given as

$$D = \begin{bmatrix} D_1 & 0 \\ 0 & D_2 \end{bmatrix} \tag{28}$$

and suppose $d = 0$, it is thus easy to get

$$\begin{aligned} \begin{bmatrix} \hat{y}_1 \\ \hat{y}_2 \end{bmatrix} &= \begin{bmatrix} G_1 & 0 \\ 0 & G_2 \end{bmatrix} \begin{bmatrix} \hat{u}_1 \\ \hat{u}_2 \end{bmatrix} \\ &= \begin{bmatrix} N_1D_1^{-1} & 0 \\ 0 & N_2D_2^{-1} \end{bmatrix} DQ\hat{r} \\ &= \begin{bmatrix} N_1Q_1 \\ N_2Q_2 \end{bmatrix} \hat{r}. \end{aligned} \tag{29}$$

We can see that the step responses of the two actuators are completely decoupled in terms of Q_1 and Q_2. As the transfer functions N_1 and N_2 have been properly designed in *step 1* to individually reflect the LM and PA closed-loop dynamics, we can then interpret Q_1 and Q_2 as the trajectory planning functions for the two actuators.

According to Theorem 1, we can infer that the minimal $\|(I - NQ)\hat{r}\|_2^2$ achievable is zero as the DSA model has no NMP zeros. This can be completed by selecting $Q_1 = N_1^{-1}$ and $Q_2 = 0$, which, however, is not a practical solution due to the improper Q_1 and the saturation of u_1. In order to compromise between the tracking speed and the limitation of the control input, we choose Q_1 and Q_2 as

$$Q_1 = N_1(0)^{-1} \tag{30}$$

$$Q_2 = \gamma N_2(0)^{-1}(1 - N_1N_1(0)^{-1}) \tag{31}$$

where $\gamma \in [0 \;\; 1]$ is a tuning scalar. It is obvious that $N_1(0)Q_1(0) = 1$ and $N_2(0)Q_2(0) = 0$, which imply that

$$y(\infty) = y_1(\infty) + y_2(\infty) = r + 0 = r. \tag{32}$$

Moreover, define the LM and PA closed-loop dynamics by

$$T_1 = N_1N_1(0)^{-1} \tag{33}$$

$$T_2 = N_2N_2(0)^{-1}. \tag{34}$$

We then have the step response transfer function of the DSA

$$T_{yr} = T_1 + \gamma T_2(1 - T_1). \tag{35}$$

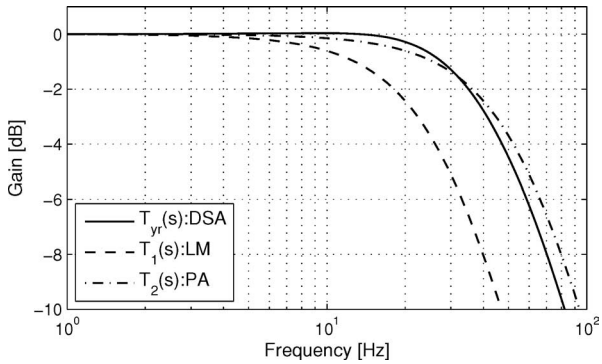

Fig. 6. Bode plot of the DSA closed-loop systems.

It is clear that when γ varies from 0 to 1, the cutoff frequency of T_{yr} switches from T_1 to that of T_2. On the other hand, we can see from (31) that the PA will follow the scaled tracking error of the LM loop, i.e., $\gamma(1 - N_1N_1(0)^{-1})r$, where γ actually determines the contribution of the PA to the overall position output. Since the PA has a faster response than the LM loop, it is preferable to have a maximal position output of the PA. Thus, we should maximize $\gamma \in [0 \;\; 1]$ subject to

$$\|T_{yr}\|_\infty \leq 1.067 \tag{36}$$

$$\|u_2\|_\infty \leq 5 \text{ V} \tag{37}$$

where the constraint (36) is introduced for an overshoot under 1 μm, while (37) is for no saturation of the PA control input. For the LM, its control input u_1 is generally not saturated for step responses within the PA range. Otherwise, we have to go back to *step 1* and reduce F_1 for slower LM dynamics. Although this iteration can be avoided by adding extra tunable dynamics to (30) to generate a slower trajectory for the LM, we believe it is not cost-effective as the selection of Q_1 as a constant gain can reduce the overall controller order.

In our case, we obtain $\gamma = 0.5$ to meet the requirement. Fig. 6 shows the Bode plot of the closed-loop systems for the DSA(T_{yr}), the LM(T_1), and the PA(T_2), respectively. We can see that the DSA frequency bandwidth is located between the LM loop and the PA loop, which indicates that the DSA servo system should be faster than the LM loop but slower than the PA loop as expected.

C. Switching Control for Step Response Beyond PA Range

For step tracking beyond the PA range, only the LM takes the control task while the PA is switched off in the initial stage. When the position output y approaches the target such that the tracking error enters the PA range, the PA is then turned on to speed up the response. At this stage, the control inputs to the two actuators are taken over by the 2-DOF controller. Such a switching control scheme is illustrated later in Fig. 7. Beyond the PA range, the LM is controlled by a proximate time-optimal controller (PTOS) [29], which can achieve near time-optimal performance and accommodate plant uncertainty and measurement noise. The LM control design beyond the PA range is not the purpose of this paper, and thus, not considered

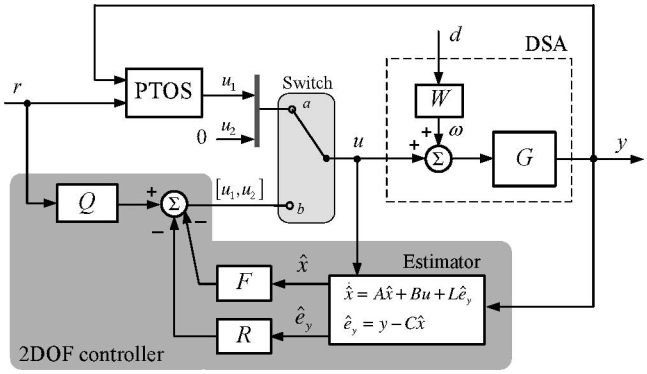

Fig. 7. DSA controller structure for practical implementation.

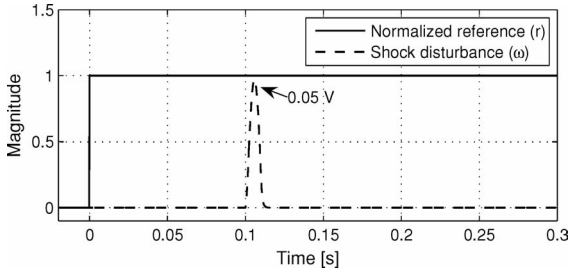

Fig. 8. Experimental reference and shock disturbance signals.

further. For alternative control design methods in this range, see [19] and the references therein.

Here, we briefly give the PTOS controller for the LM

$$u_1 = \text{sat}\big[h_2(f(e_1) - \dot{y})\big] \tag{38}$$

$$f(e_1) = \begin{cases} \dfrac{h_1}{h_2} e_1, & \text{for } |e_1| \le y_l \\ \text{sgn}(e_1)\left(\sqrt{2\bar{u}_1 k_1 \alpha |e_1|} - \dfrac{\bar{u}_1}{h_2}\right), & \text{for } |e_1| > y_l \end{cases} \tag{39}$$

$$e_1 = r - y \tag{40}$$

where sat[·] is with the saturation level of $\bar{u}_1 = 1$ V, α is referred to as the acceleration discount factor, h_1 and h_2 are constant gains, and y_l represents the size of a linear region. To make the functions $f(e_1)$ and $f'(e_1)$ continuous such that the control input remains continuous as well, we have the following constraints:

$$\alpha = \frac{2h_1}{k_1 h_2^2} \qquad y_l = \frac{\bar{u}_1}{h_1}. \tag{41}$$

The PTOS control law introduces a linear region close to the target to reduce the control chatter. In the region $|e_1| \le y_l$, the control is linear, and thus, the gains h_1 and h_2 can be designed by any linear control techniques. In our case, we select $[h_1 \;\; h_2] = [0.0024 \;\; 2.2 \times 10^{-5}]$. Thus, we have $y_l = 416$ μm.

D. Controller Implementation

Fig. 7 shows the block diagram of the DSA controller in practical implementation. When the tracking error $|r - y| > 15$ μm, the switch is with "*a*," then u_1 is generated from the PTOS controller, as given by (38), while u_2 is set to 0. When $|r - y| \le 15$ μm, the switch changes to "*b*," then the vector u is taken over by the 2-DOF controller. Note that here we use a transformed 2-DOF controller structure for easy implementation. The reason is that the lumped 2-DOF controller computed by (9) and (10) results in four subcontrollers, each with an order of 24. This high-order controller significantly increases the computation requirement for the DSP. Instead, the equivalent 2-DOF controller structure in Fig. 7 decomposes the lumped controller into several elements: each element is numerically easy to compute and appears only once in the controller. Its computational time is reduced to around one-fourth of the lumped controller. This apparently moderates the effect of computational delay that deteriorates the robustness of the closed-loop system and slows down the dynamic response of the closed-loop system to a reference command. Further, the transformed controller has better numerical accuracy, which avoids the effects of roundoff and quantization that may lead to limit-cycle oscillations in the closed-loop system.

IV. Experimental Results

Experiments are conducted on the DSA positioning system to verify the effectiveness of the proposed DSA controller. For comparison, we also carry out the experiments for the single-stage actuator control system, where the LM is controlled by the PTOS controller and the PA is switched off for any reference input. The controller is implemented by a real-time DSP system (dSPACE-DS1103) with the sampling frequency of 5 kHz. Fig. 8 shows the time signals of the step reference command as well as the shock disturbance acting on the LM. These signals are injected into the DSA control system for performance tests.

First, we obtain the tracking results within the PA range, as shown in Fig. 9. In this case, only the 2-DOF controller is at work. From Fig. 9(a), we can see that the PA is effective to speed up the step response and eliminate the LM position error due to the shock disturbance occurring at $t = 0.1$ s. As such, the dual-stage (DS) servo significantly outperforms the single-stage (SS) servo, as shown in Fig. 9(b), in terms of the settling time and disturbance rejection. Note that the high-frequency oscillations in the responses are due to the sensor quantization noise and are hard to eliminate completely. Hence, we can only guarantee the position accuracy to be within ± 1 μm. Further, we calculate the corresponding performance cost $J(e)$ defined by (1), and it is shown in Fig. 9(c), which indicates a smaller $J(e)$ achievable by the DSA compared to the single-stage servo. Although J_{opt} derived in (16) for the DSA under study can be close to 0, it is impractical due to the actuator saturation limitation. Therefore, it is used for benchmark only.

Next, we present the tracking results beyond the PA range, as shown in Fig. 10. In this case, the switching control is involved. From Fig. 10(a), we can see that the PA is activated at $t = 0.02$ s only when the tracking error is less than 15 μm. Compared with the single-stage servo in Fig. 10(b), the dual-stage servo improves the settling time only a little bit due to its small travel range relative to the reference amplitude. However, the enhancements of disturbance rejection and performance cost, as shown in Fig. 10(c), are still obvious.

Finally, we evaluate the robust performance against plant uncertainty, which mainly stems from various payloads mounting

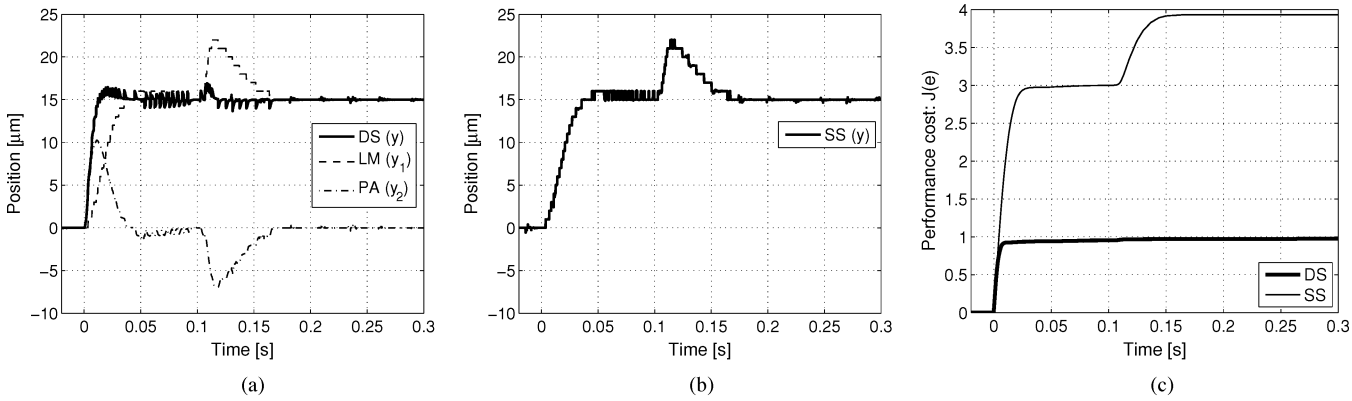

Fig. 9. Experimental 2-DOF control for disturbance rejection and step tracking within PA range. (a) DSA. (b) Single-stage actuator. (c) Performance costs.

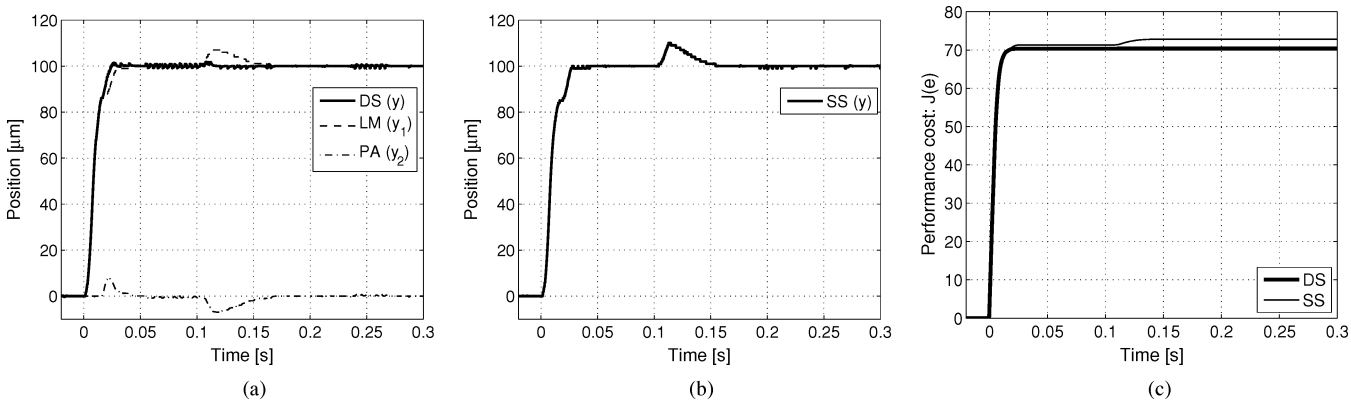

Fig. 10. Experimental switching control for disturbance rejection and step tracking beyond PA range. (a) DSA. (b) Single-stage actuator. (c) Performance costs.

TABLE 1
ROBUSTNESS EVALUATION OF THE DSA CONTROL SYSTEM

Step reference	Settling Time (ms)		Performance cost: $J(e)$	
(μm)	w/o load	w/ load	w/o load	w/ load
5	15	20	0.13	0.13
15	14	15	0.98	0.98
25	22	23	6.63	6.72
50	24	25	20.42	20.79
100	25	30	70.37	71.46

on the motor platform. Table I summaries the results for various step references and with or without 1 kg payload carried by the DSA. The results clearly show a smaller difference of the specifications between with payload and without payload. This verifies the robustness of the proposed controller on our DSA application.

V. CONCLUSION

We have revealed that the tracking and disturbance rejection problems can be decoupled into two independent optimization problems under the 2-DOF control framework. Then, each problem can be separately solved by the design of the free parameters in the 2-DOF controller, which is parameterized based on the DCF approach. The 2-DOF controller is applied to an actual DSA system for disturbance rejection and step tracking in the PA range. For long step tracking beyond the PA range, a PTOS controller is used for the LM to complete the task. Experimental results demonstrate that the proposed DSA control system can significantly speed up the step response and enhance the shock disturbance rejection compared with the single-stage servo system. Further, the performance is robust within an acceptable level when the DSA is subject to payload changes.

APPENDIX

First, from (5), the expression of K_2 (10) also equals

$$K_2 = (Y - DR)(X - NR)^{-1}. \tag{42}$$

Let the right coprime factorizations of K_2 be given by

$$K_2 = N_k D_k^{-1}. \tag{43}$$

Thus, we can take

$$N_k = Y - DR \qquad D_k = X - NR. \tag{44}$$

Next, the return difference equation $(I - GK_2)^{-1}$ can be expressed by

$$\begin{aligned}(I - GK_2)^{-1} &= (\tilde{D}^{-1}\tilde{D}D_k D_k^{-1} - \tilde{D}^{-1}\tilde{N}N_k D_k^{-1})^{-1} \\ &= (\tilde{D}^{-1}(\tilde{D}D_k - \tilde{N}N_k)D_k^{-1})^{-1} \\ &= D_k(\tilde{D}D_k - \tilde{N}N_k)^{-1}\tilde{D}. \end{aligned} \tag{45}$$

By using (5) and (44), it is straightforward to verify that

$$\tilde{D}D_k - \tilde{N}N_k = I. \tag{46}$$

Therefore, substituting (44) and (46) into (45) yields

$$(I - GK_2)^{-1} = (X - NR)\tilde{D}. \tag{47}$$

Now, by applying (47), we can easily obtain the expression of T_{yd} as

$$\begin{aligned} T_{yd} &= (I - GK_2)^{-1}GW \\ &= (X - NR)\tilde{D}\tilde{D}^{-1}\tilde{N}W \\ &= (X - NR)\tilde{N}W. \end{aligned}$$

To get the expression of T_{yr}, we only need to rewrite K_1 (9) as

$$K_1 = (D - K_2N)Q \tag{48}$$

which is expressed in terms of K_2. Applying (5) and (10) suffices to prove (48) straightforwardly, and it is thus omitted. Therefore, we have

$$\begin{aligned} T_{yr} &= (I - GK_2)^{-1}GK_1 \\ &= (I - GK_2)^{-1}G(D - K_2N)Q \\ &= \big((I - GK_2)^{-1}GD - (I - GK_2)^{-1}GK_2N\big)Q \\ &= \big((I - GK_2)^{-1}N - ((I - GK_2)^{-1} - I)N\big)Q \\ &= NQ. \end{aligned}$$

By far, we complete the proof of (12) and (13).

REFERENCES

[1] K. Mori, T. Munemoto, H. Otsuki, Y. Yamaguchi, and K. Akagi, "A dual-stage magnetic disk drive actuator using a piezoelectric device for a high track density," *IEEE Trans. Magn.*, vol. 27, no. 6, pp. 5298–5300, Nov. 1991.

[2] R. Evans, J. Griesbach, and W. Messner, "Piezoelectric microactuator for dual stage control," *IEEE Trans. Magn.*, vol. 35, no. 2, pp. 977–982, Mar. 1999.

[3] K. Chan, W. Liao, and I. Shen, "Precision positioning of hard disk drives using piezoelectric actuators with passive damping," *IEEE/ASME Trans. Mechatronics*, vol. 13, no. 1, pp. 147–151, Feb. 2008.

[4] L. Guo, D. Martin, and D. Brunnett, "Dual-stage actuator servo control for high density disk drives," in *Proc. IEEE/ASME Int. Conf. Adv. Intell. Mechatronics*, 1999, pp. 132–137.

[5] B. Kim, J. Li, and T. Tsao, "Two-parameter robust repetitive control with application to a novel dual-stage actuator for noncircular machining," *IEEE/ASME Trans. Mechatronics*, vol. 9, no. 4, pp. 644–652, Dec. 2004.

[6] S. Kwon, W. Chung, and Y. Youm, "On the coarse/fine dual-stage manipulators with robust perturbation compensator," in *Proc. IEEE Int. Conf. Robot. Autom.*, 2001, pp. 121–126.

[7] W. Yao and M. Tomizuka, "Robust controller design for a dual-stage positioning system," in *Proc. Int. Conf. Ind. Electron., Control, Instrum.*, 1993, pp. 62–66.

[8] S. Hung, E. Hwu, M. Chen, and L. Fu, "Dual-stage piezoelectric nanopositioner utilizing a range-extended optical fiber Fabry–Perot interferometer," *IEEE/ASME Trans. Mechatronics*, vol. 12, no. 3, pp. 291–298, Jun. 2007.

[9] C. Chu and S. Fan, "A novel long-travel piezoelectric-driven linear nanopositioner stage," *Precis. Eng.*, vol. 30, pp. 85–95, 2006.

[10] M. Rakotondrabe, Y. Haddab, and P. Lutz, "Voltage/frequency proportional control of stick-slip micropositioning systems," *IEEE Trans. Control Syst. Technol.*, vol. 16, no. 6, pp. 1316–1322, Nov. 2008.

[11] S. Salisbury, D. Waechter, R. Mrad, S. Prasad, R. Blacow, and B. Yan, "Design considerations for complementary inchworm actuators," *IEEE/ASME Trans. Mechatronics*, vol. 11, no. 3, pp. 265–272, Jun. 2006.

[12] S. Schroeck, W. Messner, and R. McNab, "On compensator design for linear time-invariant dual-input single-output systems," *IEEE/ASME Trans. Mechatronics*, vol. 6, no. 1, pp. 50–57, Mar. 2001.

[13] X. Huang and R. Horowitz, "Robust controller design of a dual-stage disk drive servo system with an instrumented suspension," *IEEE Trans. Magn.*, vol. 41, no. 8, pp. 2406–2413, Aug. 2005.

[14] H. Numasato and M. Tomizuka, "Settling control and performance of a dual-actuator system for hard disk drives," *IEEE/ASME Trans. Mechatronics*, vol. 8, no. 4, pp. 431–438, Dec. 2003.

[15] G. Herrmann, M. Turner, I. Postlethwaite, and G. Guo, "Practical implementation of a novel anti-windup scheme in a HDD-dual-stage servo system," *IEEE/ASME Trans. Mechatronics*, vol. 9, no. 3, pp. 580–592, Sep. 2004.

[16] T. Shen and M. Fu, "High precision and feedback control design for dual-actuator systems," in *Proc. IEEE Conf. Control Appl.*, 2005, pp. 956–961.

[17] M. Kobayashi and R. Horowitz, "Track seek control for hard disk dual-stage servo systems," *IEEE Trans. Magn.*, vol. 37, no. 2, pp. 949–954, Mar. 2001.

[18] B. Hredzak, G. Herrmann, and G. Guo, "A proximate-time-optimal control design and its application to a hard disk drive dual-stage actuator system," *IEEE Trans. Magn.*, vol. 42, no. 6, pp. 1708–1715, Jun. 2006.

[19] J. Zheng and M. Fu, "Nonlinear feedback control of a dual-stage actuator system for reduced settling time," *IEEE Trans. Control Syst. Technol.*, vol. 16, no. 4, pp. 717–725, Jul. 2008.

[20] M. Vidyasagar, *Control System Synthesis: A Factorization Approach*. Cambridge, MA: MIT Press, 1995.

[21] C. Nett, C. Jacobson, and M. Balas, "A connection between state-space and doubly coprime fractional representations," *IEEE Trans. Autom. Control*, vol. AC-29, no. 9, pp. 831–832, Sep. 1984.

[22] W. Su, L. Qiu, and I. Petersen, "Tracking performance limitations under disturbance or uncertainty," in *Proc. 16th IFAC World Congr.*, Prague, Czech Republic, 2005.

[23] J. Chen, L. Qiu, and O. Toker, "Limitations on maximal tracking accuracy," *IEEE Trans. Autom. Control*, vol. 45, no. 2, pp. 326–331, Feb. 2000.

[24] B. Chang and J. Pearson, "Optimal disturbance reduction in linear multivariable systems," *IEEE Trans. Autom. Control*, vol. AC-29, no. 10, pp. 880–887, Oct. 1984.

[25] K. Ohishi, T. Miyazaki, and Y. Nakamura, "High performance ultra-low speed servo system based on doubly coprime factorization and instantaneous speed observer," *IEEE/ASME Trans. Mechatronics*, vol. 1, no. 1, pp. 89–98, Mar. 1996.

[26] D. Wang and M. Vidyasagar, "Control of a flexible beam for optimum step response," in *Proc. IEEE Int. Conf. Robot. Autom.*, 1987, pp. 1567–1572.

[27] I. Shung and M. Vidyasagar, "Control of a flexible robot arm with bounded input: Optimum step responses," in *Proc. IEEE Int. Conf. Robot. Autom.*, 1987, pp. 916–922.

[28] M. White, M. Tomizuka, and C. Smith, "Rejection of disk drive vibration and shock disturbances with a disturbance observer," in *Proc. Amer. Control Conf.*, 1999, pp. 4127–4131.

[29] G. F. Franklin, J. D. Powell, and A. Emami-Naeini, *Feedback Control of Dynamic Systems*, 3rd ed. Reading, MA: Addison-Wesley, 1994.

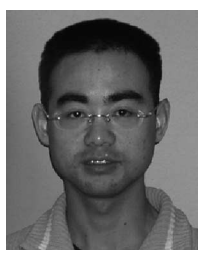

Jinchuan Zheng received the B.Eng. and M.Eng. degrees in mechatronics engineering from Shanghai Jiao Tong University, Shanghai, China, in 1999 and 2002, respectively, and the Ph.D. degree in electrical engineering from Nanyang Technological University, Singapore, in 2006.

In 2005, he joined the Australian Research Council (ARC) Centre of Excellence for Complex Dynamic Systems and Control, School of Electrical and Computer Engineering, The University of Newcastle, Newcastle, Australia, as a Research Academic. His current research interests include nanopositioning system design, vibration analysis, sensing and control, and advanced control applications in mechatronics.

Weizhou Su received the B.Eng. and M.Eng. degrees in automatic control engineering from Southeast University, Nanjing, China, in 1983 and 1986, respectively, and the Ph.D. degree in electrical engineering from The University of Newcastle, Newcastle, Australia, in 2000.

From 2000 to 2004, he was with the Department of Electrical and Electronic Engineering, Hong Kong University of Science and Technology, Hong Kong, and the School of Quantitative Methods and Mathematical Sciences (QMMS), University of Western Sydney. In 2004, he joined the College of Automation Science and Engineering, South China University of Technology, Guangzhou, China, where he is currently a Professor. His current research interests include robust control, fundamental limitations of feedback control, and signal processing.

Minyue Fu (S'84–M'87–SM'94–F'04) received the Bachelor's degree in electrical engineering from the University of Science and Technology of China, Hefei, China, in 1982, and the M.S. and Ph.D. degrees in electrical engineering from the University of Wisconsin, Madison, in 1983 and 1987, respectively.

From 1987 to 1989, he was an Assistant Professor in the Department of Electrical and Computer Engineering, Wayne State University, Detroit, MI. In 1989, he joined the Department of Electrical and Computer Engineering, The University of Newcastle, Newcastle, Australia, where he has been the Head of the Department, the Head of the School of Electrical Engineering and Computer Science, and is currently a Chair Professor in Electrical Engineering. During 1995–1996, he was a Visiting Associate Professor at the University of Iowa. During 2002, he was a Senior Fellow/Visiting Professor at Nanyang Technological University, Singapore. His current research interests include control systems, signal processing, and communications. He has been an Associate Editor of *Automatica* and the *Journal of Optimization and Engineering*.

Prof. Fu has been an Associate Editor of the IEEE TRANSACTIONS ON AUTOMATIC CONTROL.